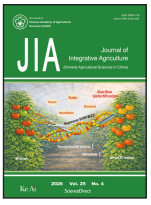
Journal of Integrative Agriculture 2026, 25(4): 1700–1715

Available online at ScienceDirect

Journal of Integrative Agriculture



RESEARCH ARTICLE

Enhancing soil organic matter mapping in saline-alkali and black soil areas with prior knowledge and multi-temporal remote sensing

Depiao Kong[1, 2], Chong Luo[1#], Huanjun Liu[1]

[1] *State Key Laboratory of Black Soils Conservation and Utilization, Northeast Institute of Geography and Agroecology, Chinese Academy of Sciences, Changchun 130102, China*

[2] *College of Geographical Sciences, Harbin Normal University, Harbin 150025, China*

Highlights

- Differentiating saline-alkali and black soil areas is crucial for accurate soil organic matter (SOM) mapping.
- Prior knowledge can be used to guide spectral index selection for each area.
- Environmental factors enhance SOM mapping: topography for the black soil area and climate for the saline-alkali area.

Abstract

Soil organic matter (SOM) monitoring using remote sensing is critical for effective land resource management and environmental protection. Mapping SOM in areas where saline and black soils are intertwined, with complex soil types and significant environmental variability, remains a challenging task. This study integrated prior knowledge and classified Jilin Province, China, into saline-alkali and black soil areas. All available Sentinel-2 images from 2019 to 2023 during the bare soil period (April to July) were collected, and the images were categorized into three time windows: day of year (DOY) 90–120, DOY 120–150, and DOY 150–180. The potentials of these time windows, spectral indices (salinity index and vegetation moisture index), environmental variables (topography and climate), and local regression models for SOM mapping in the saline-black soil transition areas were then systematically evaluated. The results revealed four key findings: (1) the optimal time window for SOM mapping in both the saline-alkali area and black soil area was DOY 90–120; (2) including the salinity index improved SOM mapping accuracy in the saline-alkali area but reduced it in the black soil area, whereas the vegetation moisture index enhanced accuracy in both areas; (3) incorporating environmental variables improved the SOM mapping accuracy in all areas, with topographic variables being more influential in the black soil area and climatic variables being more significant in the saline-alkali area; and (4) local regression models based on the saline-alkali area and black soil area outperformed the global regression model in terms of SOM mapping accuracy, although they exhibited higher uncertainty. This study demonstrates that the integration of prior knowledge and multi-temporal remote sensing images significantly enhance SOM mapping accuracy in areas where saline and black soils intersect, thus providing a scientific foundation for the precise management and protection of areas with different soil types.

Keywords: multi-temporal remote sensing, soil organic matter, prior knowledge, saline-alkali area, black soil area

1. Introduction

Soil organic matter (SOM) is an indispensable component of soils that exerts profound and essential impacts on agriculture, ecosystems, and environmental health (Lehmann and Kleber 2015; Kong *et al.* 2024). It maintains soil structure, enhances water retention, and promotes aeration (Bashir *et al.* 2021), and as the primary carbon reservoir in soils, it plays key roles in carbon cycling and climate change mitigation (Scharlemann *et al.* 2014). In addition, SOM supports plant growth and informs strategies for sustainable agriculture (Sanginga and Woomer 2009). Consequently, the accurate mapping of SOM distribution is vital for assessing agricultural productivity and carbon balance.

In studies on mapping the spatial distribution of SOM, the

Received 13 February 2025; Received in revised form 22 March 2025; Accepted 19 May 2025; Available online 2 June 2025
Depiao Kong, Mobile: +86-13883928843, E-mail: kongdepiao20000426@163.com; #Correspondence Chong Luo, E-mail: luochong@iga.ac.cn

© 2026 CAAS. Publishing services by Elsevier B.V. on behalf of KeAi Communications Co. Ltd. This is an open access article under the CC BY-NC-ND license (http://creativecommons.org/licenses/by-nc-nd/4.0/). Peer review under responsibility of Editorial Board of *Journal of Integrative Agriculture*.
doi: 10.1016/j.jia.2025.06.003

two most commonly used methods are interpolation methods and remote sensing inversion techniques (Fan *et al.* 2020; Luo *et al.* 2022). Interpolation methods, such as inverse distance weighting and radial basis function interpolation, can be used to estimate the SOM content in unsampled areas. However, interpolation methods are limited by factors such as the distribution and density dependency of sampling points (Xie *et al.* 2011). On the other hand, remote sensing inversion techniques integrate remote sensing data, ground measurements, and models (Lyu *et al.* 2021), and they offer several advantages over interpolation methods. First, remote sensing data contain multi-band information (such as vegetation indices, soil reflectance, etc.), which can enhance the accuracy of SOM content predictions (Tian *et al.* 2023). Second, remote sensing methods can integrate surface characteristics and meteorological conditions, which aids in establishing comprehensive models for SOM distribution, thereby providing deeper insights into the formation and changes of SOM (Angelopoulou *et al.* 2019). Therefore, remote sensing inversion techniques show more comprehensive and superior performance in studying the spatial distribution of SOM, particularly in large-scale regional studies and in advancing our understanding of SOM at deeper levels.

To improve the accuracy of SOM distribution maps, many scholars have employed an analytical approach based on sampled point data and integrating bare soil imagery with various environmental variables (Li *et al.* 2012; Zhang *et al.* 2021). Since areas with a higher SOM content in the soil exhibit lower spectral reflectance (Henderson *et al.* 1992; Tian *et al.* 2013), spectral information from bare soil imagery plays a crucial role in SOM estimation. However, in larger study areas, factors such as topography, climate, and policies significantly influence the timing and range of bare soil periods in agricultural lands (Schillaci *et al.* 2017). As a result, different regions within the study area may experience bare soil conditions at various times, so capturing all relevant information using short-term imagery is difficult. Therefore, relying solely on short-term agricultural bare soil imagery may not be sufficient for accurately mapping SOM distribution in the cultivated lands in Jilin Province, China. Furthermore, imagery data from a single year are often affected by extreme weather conditions, leading to significant variability (Lesk *et al.* 2016). To better meet the experimental requirements of large-scale study areas, imagery data from multiple years and periods should be analyzed to reduce the influences of random factors (Dou *et al.* 2019).

Saline soils are characterized by high concentrations of soluble salts and alkaline substances (Hayward and Wadleigh 1949), and typically exhibit elevated pH levels that can significantly hinder plant growth (Paul and Lade 2014). In contrast, black soils are rich in organic matter and have high fertility levels that are conducive to crop production (Gu *et al.* 2018). Based on soil properties and administrative divisions, prior knowledge was used to classify the study area into the saline-alkali area and the black soil area (Yu *et al.* 2021), allowing for the separate remote sensing inversion of SOM in each area. This approach can improve prediction accuracy by accounting for differences between the soil types (Song *et al.* 2016). Studies have shown that in the remote sensing inversion mapping of SOM, geographic and environmental conditions significantly influence the sensitivity and effectiveness of remote sensing indices (Matinfar *et al.* 2021; Zou *et al.* 2024; Wang *et al.* 2025). For example, integrating environmental variables and spectral bands significantly improves the prediction accuracy of SOM in arid regions (Wang Z *et al.* 2022). Zhao *et al.* (2022) successfully enhanced inversion accuracy by incorporating spectral indices in their model construction. They particularly emphasized the significance of the red-edge band in soil salinity inversion in vegetated saline-alkali areas. Furthermore, in evaluating the accuracy of SOM mapping in typical black soil areas, Luo *et al.* (2024) found that climatic covariates are of greater importance for enhancing mapping precision, given the study area's location in a plain region. In conclusion, for specific geographic and soil conditions, selecting appropriate feature variables is crucial for improving the accuracy of remote sensing inversion for SOM content (Pan *et al.* 2022).

In this study, prior knowledge refers to existing soil classification data, established spectral relationships with SOM, and insights from previous research on the environmental factors influencing SOM distribution. This information was integrated into the modeling process to refine the SOM inversion and ensure that the different soil types were analyzed separately. In addition, knowledge of the spectral indices and environmental covariates guided the selection of optimal input variables, thereby enhancing model accuracy and interpretability. Therefore, this study divided the cultivated land in Jilin Province into two areas based on their unique environmental characteristics: the saline-alkali area in the west and the black soil area in the east. Different time windows and various spectral indices were selected for each area to conduct a detailed analysis of the accuracy of SOM distribution maps for the saline-alkali area, the black soil area, and the entire cultivated land area in Jilin Province. Finally, the results were validated by comparing the highest SOM prediction accuracy from both local and global regression models, leading to the mapping of SOM content distribution in the cultivated land in Jilin Province. The specific objectives are: (1) to determine the optimal time window for SOM by combining sampling points and imagery data; (2) to evaluate the best combination of spectral indices and environmental variables that can improve accuracy within the optimal time window; and (3) to compare the accuracy of local regression and global regression, and to map the SOM content distribution of cultivated land in Jilin Province with high spatial resolution and accuracy.

2. Materials and methods

2.1. Study area

The study area is located in Jilin Province in Northeast China (121°38′–131°19′E, 40°50′–46°19′N), spanning 769.62 km from east to west and 606.57 km from north to south. The total land area is 187,400 km², accounting for 2% of China's total land area. This area has a temperate continental monsoon climate, with average annual precipitation of 400–600 mm. The average winter temperature is below −11°C,

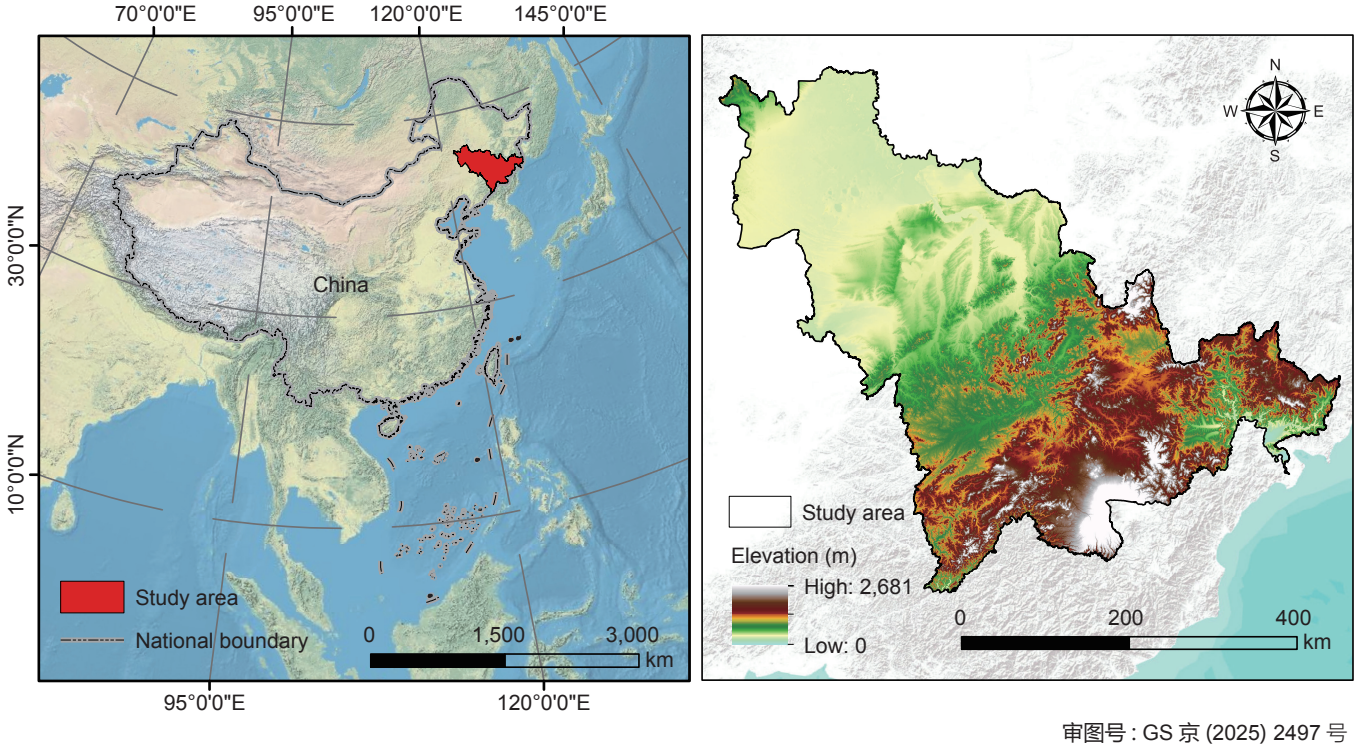
while the average summer temperature is above 23°C. Jilin Province is located in the world-renowned black soil belt, with a cultivated land area of 7.03 million hectares, accounting for approximately 37% of the province's total land area. The total amount of cultivated land ranks fifth in the nation (Guo *et al.* 2021). The cultivated land in the western part of the study area is primarily a saline-alkali area, while the eastern part is a typical black soil area. The main crops are annual crops such as corn, soybeans, and rice (Fig. 1).

2.2. Soil sample collection and processing

The soil samples used in this study were obtained from a large-scale survey conducted in Northeast China, spanning from April 2021 to May 2021. A stratified random sampling scheme was applied based on the soil type map released by the Second National Soil Survey of China to cover the various soil types. To balance the cost-effectiveness and representativeness of soil sampling with the distribution of cultivated land in the study area, major transportation routes and rural paths were used to reach the sampling locations. Soil samples were collected from cultivated land located 30–100 m away from these rural paths, while ensuring that the selected sites were not directly adjacent to major roads. A total of 210 samples were collected (Table 1; Fig. 2). In the laboratory, the collected soil samples were air-dried, ground, and sieved through a 2 mm mesh sieve (O'Kelly 2004). Subsequently, the filtered soil samples were analyzed for soil organic carbon (SOC) using the external heating potassium dichromate titration method (Nelson and Sommers 1974). Finally, the SOC content obtained was multiplied by the Van Bemmelen factor (1.724) to determine the SOM content of each soil sample (Heikkinen *et al.* 2021).

2.3. Selection and preprocessing of Sentinel-2 images

The Sentinel-2 images selected for this study were the Sentinel-2 SR images from April 1, 2019 to June 30, 2023 (day 90 to day 180). This dataset in Google Earth Engine (GEE) is labeled as "Sentinel-2 MSI: MultiSpectral Instrument, Level-2A". The code for accessing these images in GEE is "COPERNICUS/S2_SR", where "COPERNICUS" refers to the Copernicus program under the European Space Agency (ESA), and "S2_SR" indicates the Sentinel-2 surface reflectance product. This type of product typically includes quantitative measurements of surface reflectance, which are useful for various Earth observation applications such as agricultural monitoring, land cover classification, and environmental monitoring. This study used the "QA60" band to mask each image in the study area and obtain a cloud-free Sentinel-2 image collection for the specified period. According to previous research, median composite images have shown superior performance in filtering a time series, as they are less affected by extreme outliers compared to mean composites, and they have been confirmed as an effective method for obtaining the best pixels (You and Dong 2020; Wang X *et al.* 2022). A cloud-free image collection was selected from day 90 to day 180 of each year from 2019 to 2023, and the study period was divided into three time windows (DOY 90–120, DOY 120–150 and DOY 150–180) for median compositing. For band selection, ten bands (B2, B3, B4, B5, B6, B7, B8, B8A, B11 and B12) were selected as the remote sensing inputs based on previous studies, while B1 and B9 were excluded due to their lower spatial resolution (60 m) (Wang *et al.* 2021). Visible bands (B2, B3 and B4) capture soil reflectance properties, particularly in bare soil conditions, where a higher SOM content generally



审图号：GS 京 (2025) 2497 号

Fig. 1 Location and elevation map of the study area.

Table 1 Sampling information for the cultivated land in Jilin Province, saline-alkali area, and black soil area

Region	Proportion of cultivated land area (%)	Number of sampling points
Jilin Province	100	210
Saline-alkali area	37.3	50
Black soil area	62.7	160

leads to lower reflectance. Red-edge bands (B5, B6, B7 and B8A) have been widely used to assess soil moisture and salinity, both of which influence SOM distribution. The near-infrared band (B8) is sensitive to soil structure and organic matter content, while the shortwave infrared bands (B11 and B12) are particularly effective in distinguishing SOM variations and assessing soil moisture (Segarra *et al.* 2020). The combination of these bands provides a comprehensive spectral profile for SOM estimation and allows the model to capture both organic matter absorption features and environmental influences. To ensure consistency, all images were resampled to a spatial resolution of 10 m (Luo *et al.* 2023). The spectral regions and wavelength ranges of these Sentinel-2 bands are listed in Table 2.

2.4. Selection of spectral indices

Due to the presence of two distinctly different typical agricultural areas in Jilin Province, selecting suitable spectral indices for the different areas is particularly important (Fig. 3). In remote sensing mapping of saline-alkali areas, studies have shown that the salinity index (SI) and normalized difference salinity index (NDSI) can positively influence the accuracy of mapping (Khan *et al.* 2005; Allbed *et al.* 2014). In typical black soil areas, normalized difference moisture index (NDMI) and normalized difference vegetation index (NDVI) have demonstrated good explanatory power (Ayala Izurieta *et al.* 2022). Therefore, these four spectral indices were selected and categorized into salinity index and vegetation moisture index, and the band formulas shown in Table 3 were applied to the Sentinel-2 images.

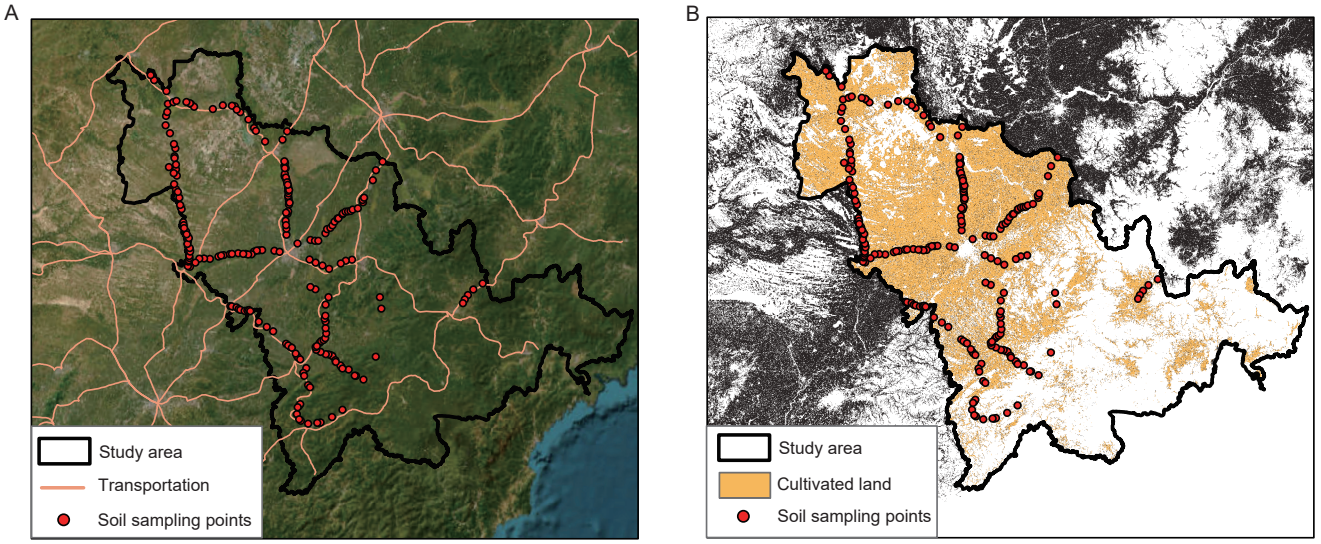
2.5. Selection and processing of environmental variables

Numerous studies have indicated that introducing environmental variables can effectively enhance mapping accuracy. Based on previous investigations, two sets of environmental variables which have been shown to significantly improve mapping accuracy (Table 4) were carefully selected, including the terrain variables of elevation and slope, and the climatic variables of multi-year average precipitation and multi-year average temperature (Wang X *et al.* 2022a; Wang Y *et al.* 2022).

Elevation data were downloaded from GEE (https://earthengine.google.com/) and processed in ArcGIS 10.8 for clipping to the extent of the study area. Slope data were calculated from the elevation data. Multi-year average precipitation and temperature data were obtained from the National Tibetan Plateau Data Centre (https://data.tpdc.ac.cn/) by selecting the monthly temperature and precipitation datasets for China from 2001 to 2020 (Peng *et al.* 2019; Peng 2020). These data were processed as multiyear averages in ArcGIS 10.8 and resampled to 10 m spatial resolution.

2.6. Partitioning the study area into two areas to achieve higher prediction accuracy

To improve the accuracy of SOM content prediction for cultivated land in Jilin Province, the study area was divided into the saline-alkali area and the black soil area based on soil characteristics (Fig. 4-A), and the remote sensing inversion of SOM content was performed separately for each area. The inversion results for the two areas were then combined to generate a spatial distribution map (i.e., local regression) of SOM for the entire study area.



审图号：GS 京 (2025) 2497 号

Fig. 2 Spatial distribution of sampling points in the study area. A, sampling points along major transportation routes. B, sampling points based on the main distribution areas of cultivated land.

Table 2 Spectral information of selected Sentinel-2 bands in this study

Description	Band name	Wavelength (nm)	Resolution (m)
Blue	B2	496.6	10
Green	B3	560.0	10
Red	B4	664.5	10
Red Edge 1	B5	703.9	20
Red Edge 2	B6	740.2	20
Red Edge 3	B7	782.5	20
NIR	B8	835.1	10
Red Edge 4	B8A	864.8	20
SWIR 1	B11	1,613.7	20
SWIR 2	B12	2,202.4	20

In this study, local regression refers to creating separate regression models for different areas with distinct soil characteristics (saline-alkali area and black soil area) to better capture regional heterogeneity. On the other hand, global regression refers to applying a single regression model to the entire study area, which assumes that the relationship between variables is similar across the entire region.

As shown in the boxplot in Fig. 4-B, the SOC content of soil samples in the saline-alkali area is generally lower than in the black soil area, indicating that regional heterogeneity should be considered in the model. Given the differential distribution patterns of SOC content in the saline-alkali area and black soil area, local regression is better suited to the specific characteristics of each area, potentially improving model accuracy. By accounting for these regional differences, local regression can more effectively capture heterogeneous features and reduce model errors, thereby enhancing the accuracy and applicability of the model. To evaluate the effectiveness of local regression in improving prediction accuracy, a comparative analysis was conducted between the global regression and the local regression to identify the most suitable modeling approach for predicting SOM content in cultivated land across Jilin Province.

2.7. Random forest regression

The random forest regression model constructs an ensemble of multiple decision trees by randomly selecting training samples and features, thereby creating diverse tree models. The final prediction of the model is the average of the predictions from all trees. This ensemble method enhances the model's robustness and prediction accuracy (Zhou *et al.* 2020). Random forests excel in handling high-dimensional data and mitigating overfitting issues, which is why they are widely applied to regression problems (Shah *et al.* 2019). Drawing from previous research and through extensive experimentation, the number of decision trees was set to 400. Experimental validation demonstrated that this value ensures sufficient accuracy while preventing overfitting. For the remaining model parameters, values were selected based on prior knowledge and repeated testing to optimize performance (Luo *et al.* 2024).

2.8. Accuracy verification

This study employed five-fold cross-validation to assess the model's accuracy. This method involves randomly dividing the data into five subsets, ensuring a balance between comprehensiveness, robustness, and computational cost through repeated evaluations with different data partitions (Akpokiro *et al.* 2022). In each round of the five-fold cross-validation, four subsets are used for training the model, while the remaining subset is used to validate the model's performance. This process is repeated five times, ensuring that each subset serves as the validation set once, and ultimately yielding five performance evaluation results. The accuracy of each model was evaluated using the coefficient

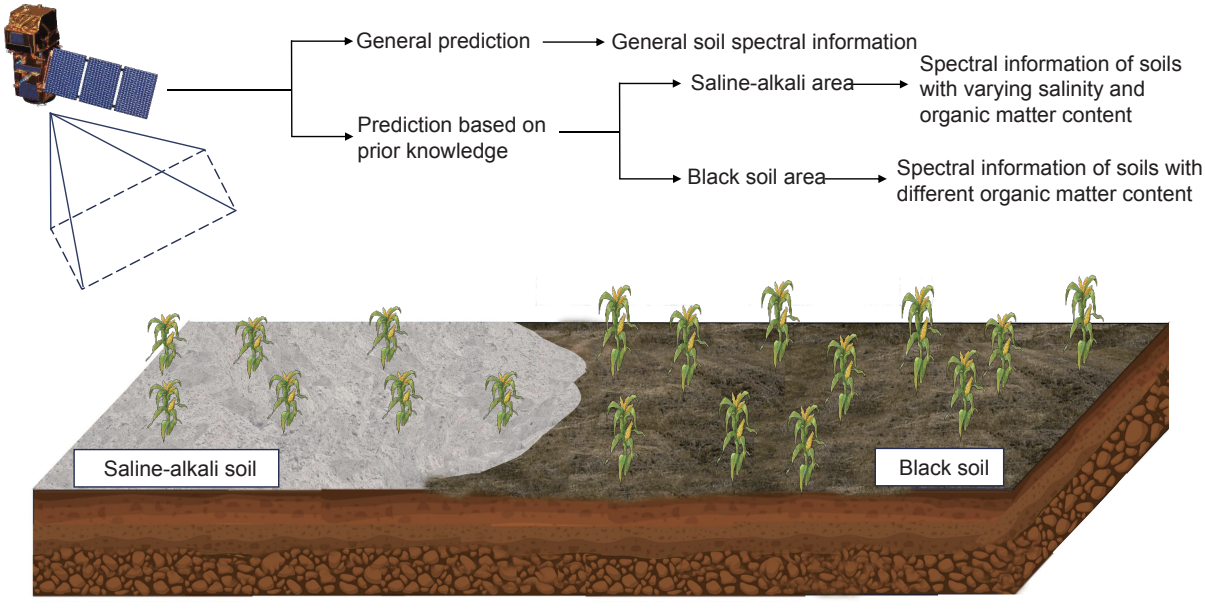


Fig. 3 Selection of spectral information based on prior knowledge combined with distinctions between the saline-alkali and black soil areas.

Table 3 Band calculation formulas for the spectral indices in Sentinel-2

Category	Spectral index	Band formula
Salinity index	Salinity index	$SI=\sqrt{B2\times B4}$
Vegetation moisture index	Normalized difference salinity index	NDSI=(B4–B8)/(B4+B8)
	Normalized difference moisture index	NDMI=(B8–B11)/(B8+B11)
	Normalized difference vegetation index	NDVI=(B8–B4)/(B8+B4)

Table 4 Relevant information for environmental variables

Category	Environmental variable	Code	Type
Topography	Elevation	DEM (m)	Grid
	Slope	SLOPE (°)	Grid
Climate	Precipitation	PRE (mm)	Grid
	Temperature	TEMP (°C)	Grid

of determination (R^2) and root mean square error (RMSE) (Williams 1987). The formulas are as follows:

$$R^2=1-\frac{\sum_{i=1}^{n}(y_i-\hat{y}_i)^2}{\sum_{i=1}^{n}(y_i-\bar{y}_i)^2} \quad (1)$$

$$RMSE=\sqrt{\frac{1}{n}\sum_{i=1}^{n}(y_i-\hat{y}_i)^2} \quad (2)$$

where n represents the number of samples, y_i represents the observed value at the i-th sampling point, and $\hat{y}_i$ represents the measured value at the i-th sampling point. Usually, the value of R^2 ranges from 0 to 1. When the value of R^2 is close to 1, it indicates that the predicted value of the model is closer to the actual measured value. On the other hand, the RMSE is used to assess the difference between the actual measured value and the predicted value, so a smaller RMSE value indicates that the model inversion is more accurate and the difference between the two is smaller.

2.9. Uncertainty analysis of predictive results

In this study, five-fold cross-validation and random forest regression models were applied to the saline-alkali and black soil areas, yielding five validation results. Uncertainty analysis is a crucial step in determining the credibility of predictions (Goidts *et al.* 2009). Therefore, the five validation results from the saline-alkali area and black soil area were combined to calculate their standard deviation (absolute error) and coefficient of variation (relative error). This approach was used to assess the uncertainty of the predictive model when mapping SOM content in the saline-alkali area and black soil area.

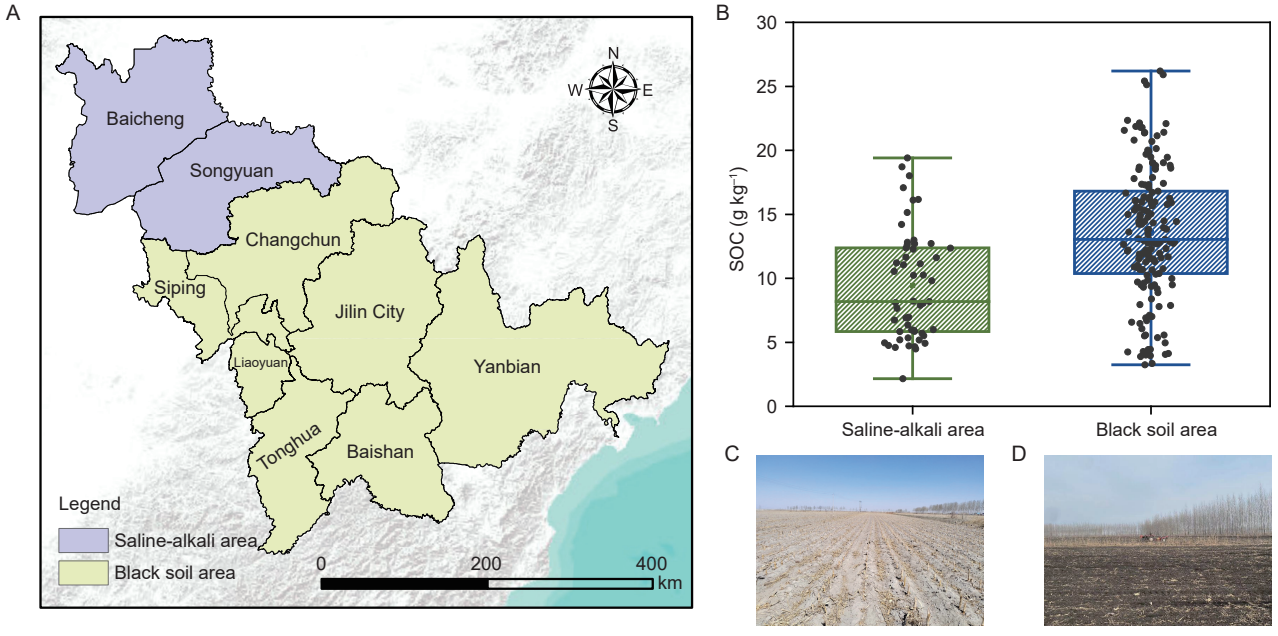
2.10. Technology roadmap

The technology roadmap for this study is depicted in Fig. 5.

3. Results

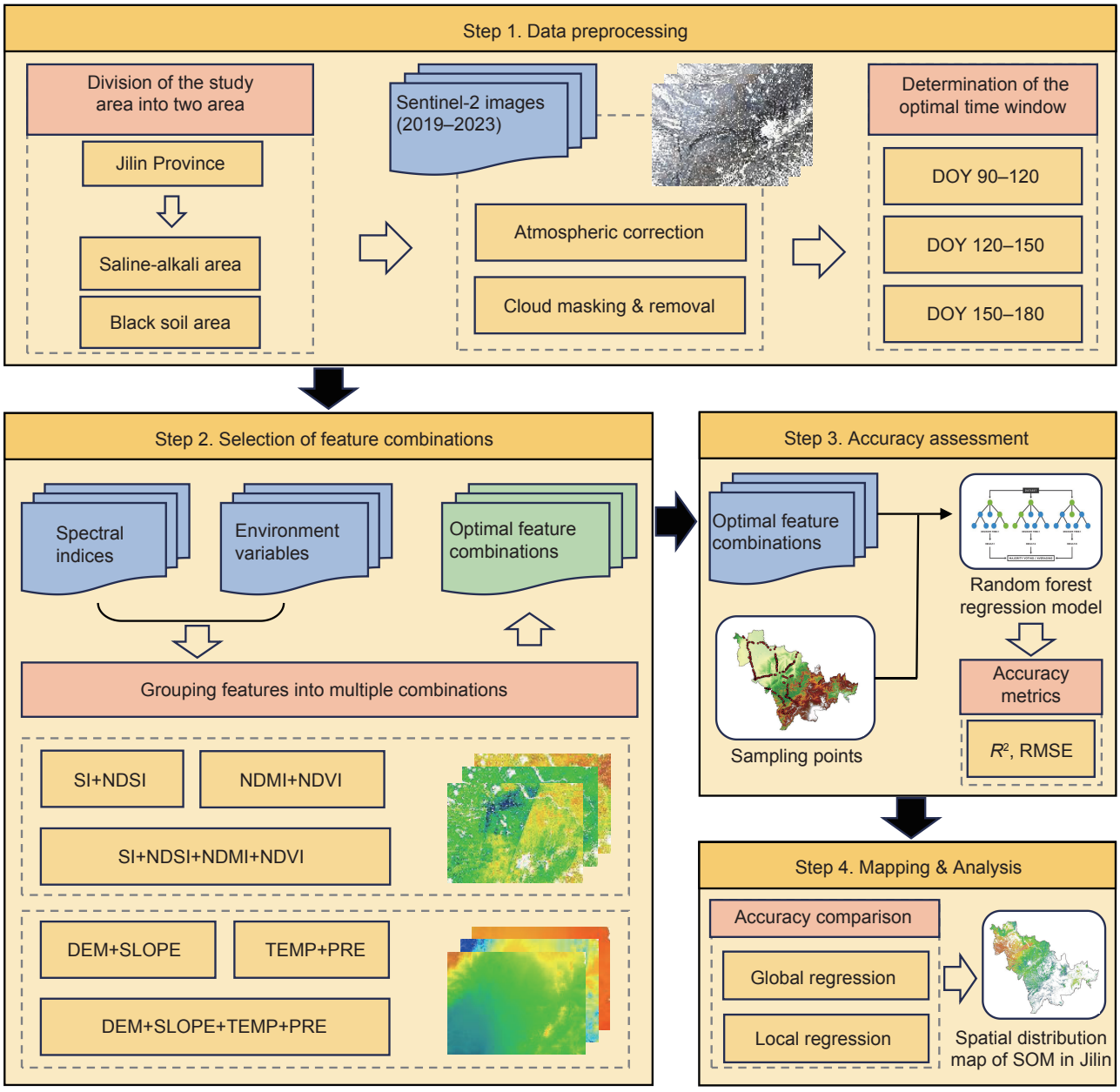
3.1. Spectral curve differences among soils with different SOM contents

Fig. 6 illustrates the spectral reflectance characteristics of agricultural soils with different SOM content levels in the saline-alkali area and black soil area. A similar trend in the spectral curves was observed for both areas, where higher



审图号：GS 京 (2025) 2497 号

Fig. 4 Study area divisions and supporting evidence for local regression modeling. A, schematic map of the study area divisions. B, boxplot of soil sample data for the saline-alkali and black soil areas. C, field photograph of the saline-alkali area, taken in April 2023. D, field photograph of the black soil area, taken in April 2023.



审图号 : GS 京 (2025) 2497 号

Fig. 5 Technology roadmap of this study.

SOM content correlated with lower soil spectral reflectance. Moreover, reflectance generally increased with wavelength, except for slight reductions observed in the NIR to Red Edge 4 and SWIR 1 to SWIR 2 ranges.

In the saline-alkali area and black soil area, the spectral reflectance of soils with SOM content<10 g kg^{-1} are nearly identical. However, when the SOM content ranges between 10 and 20 g kg^{-1}, the spectral reflectance of saline-alkali area soils is notably higher than that of black soil area soils. For SOM contents between 20 and 30 g kg^{-1}, the spectral reflectance of saline-alkali area soils shows minimal differences from the black soil area soils before Red Edge 4, but significantly higher reflectance is observed in the SWIR 1 to SWIR 2 range. Since the SOM content in the saline-alkali area is generally less than 30 g kg^{-1}, comparisons beyond an SOM content of >30 g kg^{-1} are not feasible based on the spectral curve characteristics.

3.2. Mapping accuracy of SOM at different time windows

This study first explored the optimal time window for mapping SOM in Jilin Province using remote sensing. Table 5 shows that the optimal time window for SOM mapping in the saline-alkali area, black soil area, and the Jilin Province is DOY 90–120. Significant differences in SOM prediction accuracy were observed for the other time windows. In the saline-alkali area, SOM mapping accuracy initially decreased and then increased over time, while in the black soil area and Jilin Province overall, SOM mapping accuracy consistently

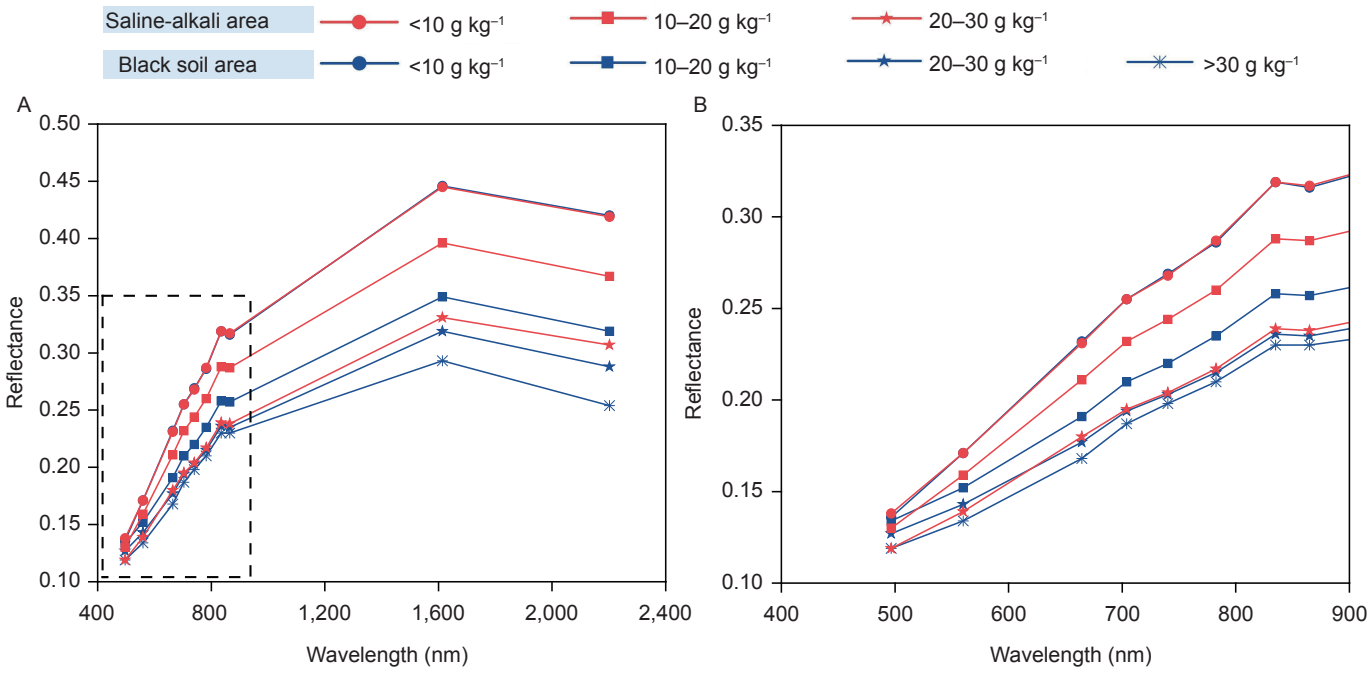


Fig. 6 Spectral reflectance characteristics of soils with different soil organic matter (SOM) contents in the saline-alkali and black soil areas. A, spectral curve characteristics of soils with different SOM contents using Sentinel-2. B, detailed information on the spectral curves for different SOM contents in the saline-alkali and black soil areas prior to Red Edge 4.

Table 5 Soil organic matter prediction accuracy of synthetic images in different time windows

Region	DOY 90–120[1)]		DOY 120–150		DOY 150–180	
	R^2	RMSE (g kg^{-1})	R^2	RMSE (g kg^{-1})	R^2	RMSE (g kg^{-1})
Jilin Province	0.555	3.474	0.500	3.682	0.417	3.980
Saline-alkali area	0.644	2.445	0.523	2.849	0.577	2.669
Black soil area	0.480	3.730	0.427	3.915	0.365	4.119

[1)] DOY, day of year.

declined as time progressed.

3.3. SOM prediction accuracy after adding spectral indices

Three sets of spectral index combinations were tested in the prediction model: salinity index (SI+NDSI), vegetation moisture index (NDMI+NDVI), and salinity index+vegetation moisture index (SI+NDSI+NDMI+NDVI). The results (Table 6) show that SOM prediction accuracy significantly improved across all areas after incorporating the spectral indices. Specifically, the saline-alkali area and Jilin Province demonstrated the most notable enhancements in accuracy with the inclusion of SI+NDSI+NDMI+NDVI. In contrast, the black soil area showed a slight reduction in R^2 by 0.002 and an increase in RMSE by 0.006 g kg^{-1} after adding SI+NDSI. However, the accuracy improved most significantly after adding NDMI+NDVI alone, with an increase in R^2 of 0.033 and a reduction in RMSE of 0.122 g kg^{-1}. This indicates that targeted inclusion of spectral indices does indeed enhance accuracy, while the inclusion of ineffective spectral indices may reduce accuracy.

Table 6 Soil organic matter prediction accuracy after adding spectral indices for the optimal time window (DOY 90–120)[1)]

Region	Spectral indices	R^2	RMSE (g kg^{-1})
Jilin Province	SI+NDSI	0.561	3.451
	NDMI+NDVI	0.575	3.394
	SI+NDSI+NDMI+NDVI	0.576	3.389
Saline-alkali area	SI+NDSI	0.656	2.399
	NDMI+NDVI	0.654	2.407
	SI+NDSI+NDMI+NDVI	0.657	2.397
Black soil area	SI+NDSI	0.478	3.736
	NDMI+NDVI	0.513	3.608
	SI+NDSI+NDMI+NDVI	0.504	3.640

[1)] DOY, day of year; SI, salinity index; NDSI, normalized difference salinity index; NDMI, normalized difference moisture index; NDVI, normalized difference vegetation index.

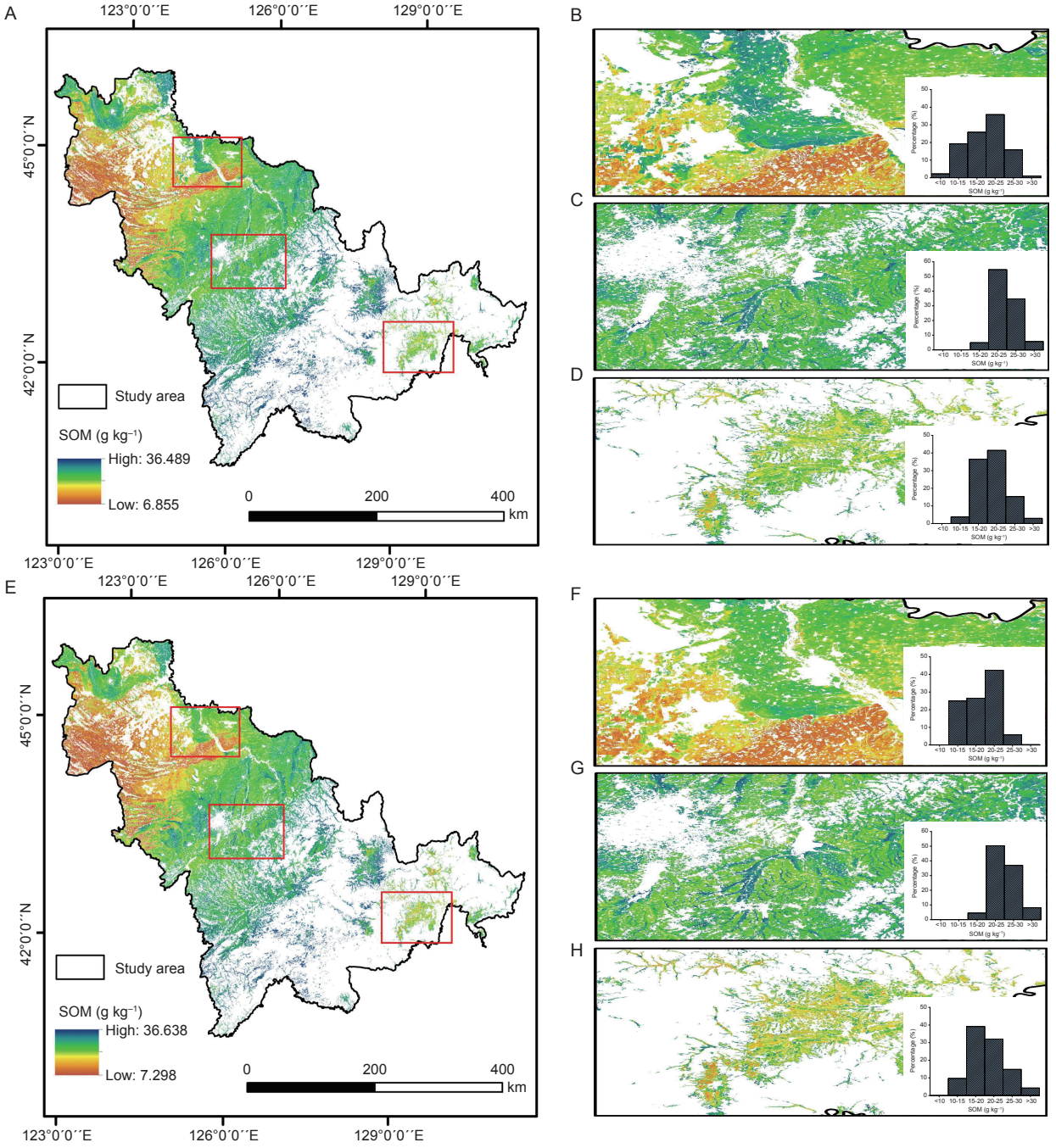
Table 7 Soil organic matter prediction accuracy after adding environmental variables using the best spectral indices (DOY 90–120)[1)]

Region	Environment variables	R^2	RMSE (g kg^{-1})
Jilin Province	DEM+SLOPE	0.610	3.252
	TEMP+PRE	0.613	3.243
	DEM+SLOPE+TEMP+PRE	0.617	3.222
Saline-alkali area	DEM+SLOPE	0.666	2.367
	TEMP+PRE	0.678	2.326
	DEM+SLOPE+TEMP+PRE	0.686	2.300
Black soil area	DEM+SLOPE	0.548	3.480
	TEMP+PRE	0.530	3.545
	DEM+SLOPE+TEMP+PRE	0.551	3.466

[1)] DOY, day of year; DEM, elevation; SLOPE, slope; TEMP, temperature; PRE, precipitation.

3.4. SOM prediction accuracy after adding environment variables

After determining the time windows and spectral indices with the highest accuracy, the environmental variables were categorized into three combinations: topography, climate, and topography+climate. The results (Table 7) demonstrate an overall improvement in the SOM prediction models across all areas with the inclusion of environmental variables. The combination of topography+climate yielded the most significant accuracy enhancement, indicating a combined influence of topographic and climatic variables on the spatial distribution of SOM in all three areas. Specifically, by using this combination, the R^2 values increased by 0.041 with a corresponding RMSE reduction of 0.167 g kg^{-1} for Jilin Province; R^2 increased by 0.029 with an RMSE reduction of 0.097 g kg^{-1} for the saline-alkali area; and R^2 increased by 0.038 with an RMSE reduction of 0.142 g kg^{-1} for the black soil area. In addition, when the environmental



审图号 : GS 京 (2025) 2497 号

Fig. 7 Comparison of the soil organic matter (SOM) spatial distributions predicted by global and local regression models in Jilin Province, China. A, SOM spatial distribution map from the global regression. B–D, typical regions selected from A. E, SOM spatial distribution map from the local regression. F–H, typical areas selected from E. The bar charts in B–D and F–H represent the proportions of different SOM contents within the respective areas.

variables were included separately, the climatic variables contributed more significantly to SOM prediction accuracy in Jilin Province and the saline-alkali area, whereas topography provided higher predictive accuracy for the black soil area.

3.5. Mapping results of SOM

In this study, the data from the SOM prediction models with the highest accuracy from local regression were pooled. The results show that the R^2 value of the prediction model after integrating local regression is 0.622, which is higher than the R^2 value of the global regression SOM prediction model (0.617), indicating that local regression offers higher prediction accuracy. Based on this, local regression was applied to map the SOM predictions for the saline-alkali area and black soil area, which yielded more accurate results than those obtained from the global regression in Jilin Province. To examine the spatial distribution differences between global regression and local regression, three representative areas were randomly selected based on the distribution of sampling points and the regional characteristics of the northern, central, and southern parts of the study area (Fig. 7-B–D and F–H).

As shown in Fig. 7, the spatial distribution map of SOM content highlights the characteristics of SOM distribution across Jilin Province and its typical areas. The average SOM content in Jilin Province was 21.92 g kg^{-1}, with 17.05 g kg^{-1} in the saline-alkali area and 24.58 g kg^{-1} in the black soil area. Overall, the SOM content in Jilin Province exhibited a spatial pattern of lower levels in the northwest, with a gradual increase from the center to the southeast (Fig. 7-A and E). In the saline-alkali area, the SOM content was relatively low in the southern and central areas but higher in the east and north. In the black soil area, the SOM content showed an increasing trend from northwest to southeast. In the global regression predictions (Fig. 7-B and D), the SOM contents in the northern and southern areas were higher than those predicted by local regression (Fig. 7-F and H), whereas the two regression methods produced similar predictions in the central part of the study area (Fig. 7-C and G). Furthermore, the proportions of cultivated land with SOM content greater than 20 g kg^{-1} were different in the three typical areas. In the global regression, the percentages of cultivated land with an SOM content above 20 g kg^{-1} were higher in the north and south compared to the local regression, while the percentages in the central area were roughly the same (Fig. 7-B–D and F–H).

3.6. Uncertainty analysis

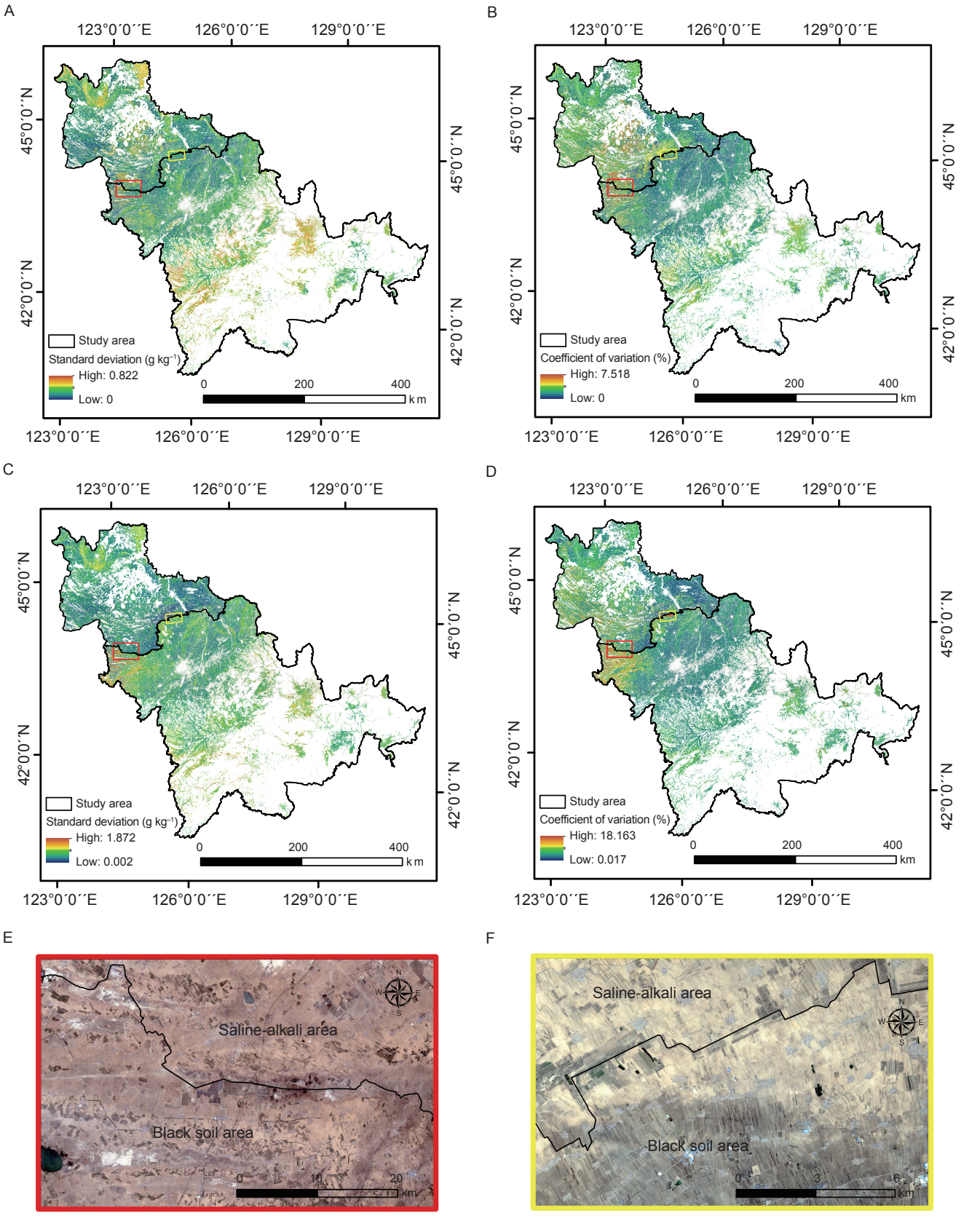
Fig. 8 presents the uncertainty analysis results for both the global regression and local regression. In the global regression, the standard deviation of the assessment metrics ranged from 0 to 0.82 g kg^{-1}, and the coefficient of variation varied from 0 to 7.52%. The mean standard deviation was 0.19 g kg^{-1}, and the mean coefficient of variation was 1.63% (Fig. 8-A and B). In contrast, for the local regression, the standard deviation ranged from 0 to 1.87 g kg^{-1}, while the coefficient of variation ranged from 0.02 to 18.16%. The mean standard deviation was 0.39 g kg^{-1}, and the mean coefficient of variation was 3.22% (Fig. 8-C and D). Thus, the global regression metrics exhibited lower standard deviations and coefficients of variation, indicating that its predictions fluctuated less within the areas. However, the local regression was more effective in capturing regional differences, resulting in higher adaptability of the model within each area. This approach better aligns with the environmental characteristics of the study area, which is expected to enhance the model's prediction accuracy.

In addition, the imagery analysis revealed a significant number of uncertain transitional zones where saline-alkali soil gradually transforms into black soil in the transition areas between these two areas (Fig. 8-E and F). This could explain the higher uncertainty observed in the local regression model relative to the global regression. These results highlight the limitations of delineating the saline-alkali and black soil areas based solely on administrative boundaries. These findings suggest that a more precise classification based on the actual soil type distribution is essential for improving model performance and reducing the uncertainty in transitional areas.

4. Discussion

4.1. Selection of specific time windows

In this study, the bare soil period was divided into three time windows. Preliminary experiments indicated that the period from DOY 90–120 provides the highest accuracy for SOM inversion, possibly due to the moderate suitability of soil moisture during this time. However, further investigations are needed to explore this finding in more detail (Table 8). Such findings could help to refine the optimal time window for SOM remote sensing retrieval in future studies. During DOY 90–120, the averages and standard deviations of NDVI and NDMI in Jilin Province were lower compared to the other two time windows. Although NDVI values are typically low in bare soil areas, suggesting minimal vegetation cover, this time window (DOY 90–120) corresponds to the peak bare soil period in Jilin Province, where the soil is mostly exposed. This minimal vegetation cover enhances the sensitivity of remote sensing data to SOM, as the signal from soil properties such as organic matter content is less obscured by vegetation. This interpretation applies to temporal variations during the bare soil period. In contrast, the higher NDVI and NDMI values observed in black soil areas reflect spatial differences in vegetation and moisture conditions, which are indicative of environments with typically higher SOM levels. Moreover, this period occurs in the spring when generally favorable lighting conditions contribute to improving the quality and resolution of remote sensing images (Richardson *et al.* 2007), thereby enhancing the accuracy of SOM remote sensing retrieval. For example, Luo *et al.* (2024) found that imagery collected in May (DOY 120–150) significantly improved the accuracy for their study area in the Sanjiang Plain of Heilongjiang Province. Considering that Jilin Province is located at a relatively southern latitude, its snow and ice melt earlier in the season (Yang *et al.* 2022). Spring plowing activities, either ongoing or completed, would have exposed much of the farmland as bare soil. Therefore, the time window with optimal accuracy may correspondingly advance. This inference is based on reasonable assumptions about the geographical location and climatic conditions, and



审图号：GS 京 (2025) 2497 号

Fig. 8 Standard deviations and coefficients of variation for soil organic matter (SOM) mapping using global and local regressions. A, standard deviation for global regression. B, coefficient of variation for global regression. C, standard deviation for local regression. D, coefficient of variation for local regression. E, image from Sentinel-2 at the junction of the saline-alkali area and the black soil area taken in April 2023 (red box on the left). F, image from Sentinel-2 at the junction of the saline-alkali area and the black soil area taken in April 2023 (yellow box on the right).

Table 8 Normalized difference vegetation index (NDVI) and normalized difference moisture index (NDMI) information for Jilin Province in the different time windows

Index	Time window	Average value	Maximum value	Minimum value	Standard deviation
NDVI	DOY 90–120	0.168	0.772	–0.440	0.049
	DOY 120–150	0.209	0.873	–0.551	0.129
	DOY 150–180	0.361	0.930	–0.618	0.172
NDMI	DOY 90–120	–0.147	0.873	–0.391	0.055
	DOY 120–150	–0.079	0.738	–0.417	0.116
	DOY 150–180	–0.009	0.855	–0.439	0.159

Table 9 Average values of spectral indices in the saline-alkali area and the black soil area in the different time windows[1)]

Area	Time window	SI	NDSI	NDMI	NDVI
Saline-alkali area	DOY 90–120	0.153	–0.161	0.162	0.161
	DOY 120–150	0.173	–0.173	–0.098	0.173
	DOY 150–180	0.131	–0.288	–0.058	0.288
Black soil area	DOY 90–120	0.141	–0.171	–0.140	0.171
	DOY 120–150	0.155	–0.229	–0.069	0.229
	DOY 150–180	0.106	–0.399	0.017	0.399

[1)] SI, salinity index; NDSI, normalized difference salinity index; NDMI, normalized difference moisture index; NDVI, normalized difference vegetation index.

provides a potentially more accurate timing choice for the study.

4.2. Impact of specific spectral indices on the accuracy of SOM prediction models in the saline-alkali area and black soil area

As more remote sensing data becomes available, integrating multiple spectral indices to improve remote sensing mapping accuracy has proven to be effective (Chen *et al*. 2017; Shafizadeh-Moghadam *et al.* 2022). However, the accuracy of remote sensing mapping in different regions may vary with the same spectral indices (Žížala *et al.* 2019). This study found that the application of SI+NDSI improved the model's predictive accuracy in the saline-alkali area but resulted in reduced accuracy in the black soil area. This phenomenon can be explained by the high salt content in the saline-alkali area, where SI+NDSI performed well since it is highly sensitive to salt (Dong *et al.* 2020). In contrast, the salt content is low in the black soil area, so SI+NDSI may fail to effectively capture the soil characteristics, leading to a decline in model performance (Fig. 9).

As shown in Table 9, the SI and NDSI values in the saline-alkali area are consistently higher than those in the black soil area across all three time windows, indicating higher salinity in the saline-alkali area. Conversely, the NDMI and NDVI values in the black soil area are greater than those in the saline-alkali area, suggesting that NDMI and NDVI are more beneficial for improving the accuracy of SOM remote sensing mapping in the black soil area. Jilin Province receives ample precipitation, and the SOM levels in both saline-alkali and black soil areas show sensitive responses to the commonly used indices of NDMI and NDVI, effectively enhancing the model's accuracy after remote sensing inversion. As shown in Fig. 10, the SI and NDSI values exhibit significant differences and notable variation trends between the saline-alkali and black soil areas during DOY 90–120. However, the changes in SI and NDSI are smoother in the other two time windows. This observation further validates the rationale for selecting DOY 90–120 as the study period.

4.3. Influence of environmental variables on SOM prediction accuracy in different areas

The differential impacts of environmental variables on SOM prediction accuracy in the two areas can be attributed to their distinct geomorphological characteristics and climatic variability (Fig. 11). In the saline-alkali area, elevation and slope exhibit minimal variation (Fig. 11-A and B), indicating a relatively homogeneous topographic landscape. Under such conditions, topographic variables contribute little additional explanatory power to SOM modeling (Qin *et al.* 2012). Instead, climatic variables, particularly precipitation and temperature, play a more dominant role in improving prediction accuracy. Precipitation directly regulates soil moisture availability, thus influencing organic matter decomposition, leaching, and accumulation (Daly and

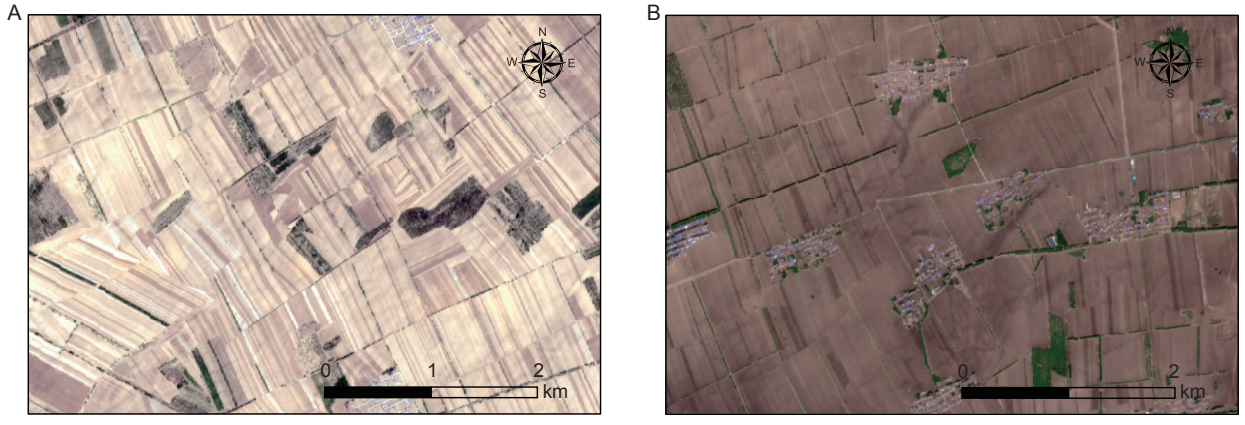
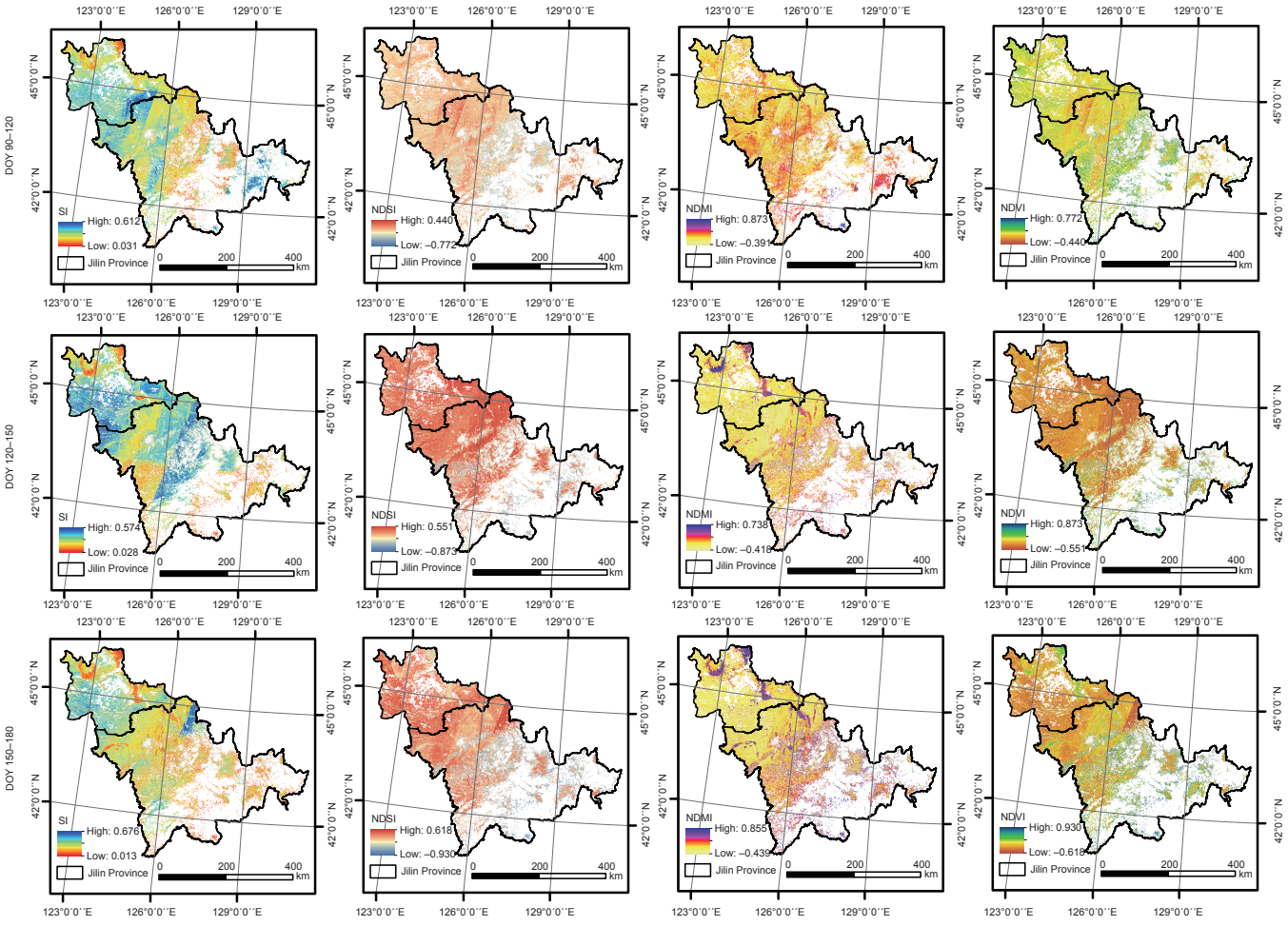


Fig. 9 Sentinel-2 imagery of representative regions in the saline-alkali area and black soil area. A, Sentinel-2 image of the saline-alkali area, taken in May 2023. B, Sentinel-2 image of the black soil area, taken in May 2023.



审图号：GS 京 (2025) 2497 号

Fig. 10 Spatial distribution maps of the spectral indices in Jilin Province for the three time windows. DOY, day of year; SI, salinity index; NDSI, normalized difference salinity index; NDMI, normalized difference moisture index; NDVI, normalized difference vegetation index.

Porporato 2005). While excessive rainfall can lead to nutrient loss, moderate levels promote microbial activity and organic matter input (Zeglin *et al.* 2013). Temperature further modulates microbial activity and decomposition rates, where higher temperatures accelerate organic matter breakdown, while lower temperatures favor SOM accumulation (Curtin *et al.* 2012; Sihi *et al.* 2016; Zhou *et al.* 2024). Given that the saline-alkali area exhibits a relatively uniform precipitation pattern, these climatic factors collectively enhance the SOM prediction accuracy, making climatic variables the most influential predictors in this region.

In contrast, the black soil area exhibits substantial topographic heterogeneity, particularly in the eastern mountainous regions where the elevation and slope vary considerably (Fig. 11-A and B). In such landscapes, topography plays a critical role in controlling soil redistribution, hydrological processes, and erosion dynamics (Fu *et al.* 2011; Dialynas *et al.* 2016; Yu *et al.* 2020), all of which directly impact SOM accumulation and decomposition. In addition, the spatial variability of precipitation in the black soil area is greater than in the saline-alkali area (Fig. 11-C and D), leading to complex interactions between topographic and climatic factors. Under these conditions, incorporating topographic variables provides essential supplementary information that contributes more significantly to model accuracy improvement than the climatic variables alone.

These findings highlight the necessity of region-specific variable selection when modeling SOM distribution. In relatively flat and topographically uniform areas, climatic variables serve as the primary predictors of SOM variability. Conversely, in regions with complex geomorphological features, topographic factors play a more dominant role. Future research should consider integrating additional hydrological and land-use parameters to further refine the SOM prediction models across diverse landscapes.

4.4. Limitations and prospects

This study used synthesized multi-year Sentinel-2 images for DOY 90–120, combined with various spectral indices and environmental variables, to map the SOM content distribution in Jilin Province's cultivated lands. This approach has demonstrated effectiveness in predicting large-scale SOM content maps. However, some scholars have found that

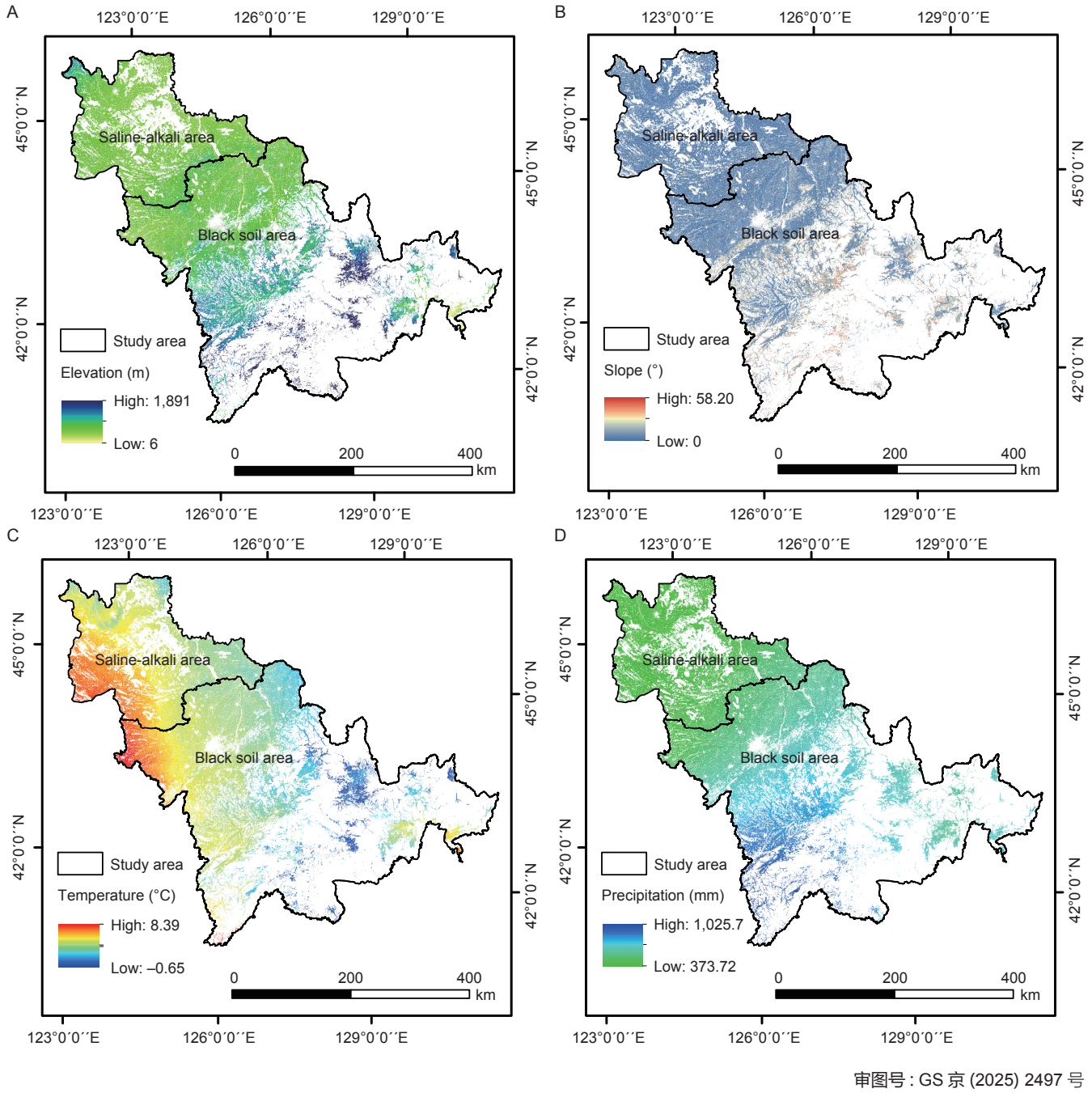


Fig. 11 Spatial distributions of four environmental variables in the cultivated land of the study area. A, elevation. B, slope. C, annual mean temperature. D, annual mean precipitation.

using synthesized images at 20-day intervals can achieve the best prediction accuracy for mapping the distribution of SOM in larger study areas (Luo *et al.* 2023). The Sentinel-2 satellite collects ground data every five days, allowing for the selection of single-date or composite images spanning multiple dates. The 30-day interval used for composite images in this study may be either too long or too short to fully capture the changes in surface conditions. In a specific study area, selecting the appropriate interval for composite images is crucial for achieving the research objectives.

Studies have shown that adding 16 salt indices in an saline-alkali area significantly improves the accuracy of bare soil inversion and demonstrates a strong correlation (Zhao *et al.* 2022). This study selected two salt indices, which did significantly improve the prediction accuracy of SOM. Given this finding, future studies should explore more salt indices to further enhance the inversion accuracy of SOM distribution maps in saline-alkali agricultural areas. Studies have found that human factors such as land use practices and land management measures can play a crucial role in the spatial distribution of SOM content (Zhao *et al.* 2023). Therefore, incorporating human factors as environmental variables should be considered in future research to enhance the prediction accuracy of SOM content.

The uncertainty analysis in this study mainly focused on the standard deviation and coefficient of variation, but did not explore the root causes of uncertainty in detail. Future research should address this limitation by investigating factors such as data variability, model parameter choices, and the complexity of environmental transitions between the saline-alkali and black soil areas. In particular, integrating higher-resolution data, considering alternative modeling approaches, and exploring uncertainty quantification methods could reduce the uncertainty in future SOM prediction models (Post *et al.* 2008).

5. Conclusion

In this study, the optimal time window of DOY 90–120 was identified for SOM remote sensing in the saline-alkali area and black soil area of Jilin Province. The results indicate that the salinity index enhances SOM mapping accuracy in the saline-alkali area but reduces accuracy in the black soil area, highlighting the importance of selecting an index that is appropriate for the specific soil properties. Integrating topographic and climatic variables significantly enhanced mapping accuracy, with climatic factors playing a key role in the saline-alkali area and topography being crucial in the black soil area. In addition, the local regression model outperformed the global model, offering valuable insights for large-scale SOM mapping. These findings contribute to the development of high-resolution SOM maps and can support improvements in agricultural management and productivity.

Acknowledgements

This study was supported by the Science and Technology Development Plan Project of Jilin Province, China (20240602052RC). Sincere thanks to the anonymous reviewers and members of the editorial team for their comments and contributions.

Declaration of competing interest

The authors declare that they have no conflict of interest.

Declaration of generative AI and AI-assisted technologies in the writing process

During the preparation of this manuscript, the authors used ChatGPT 4.0 to assist in improving the clarity and readability of the language. All content generated was carefully reviewed and revised by the authors as necessary, and the authors take full responsibility for the final content of the article.

References

Akpokiro V, Martin T, Oluwadare O. 2022. EnsembleSplice: Ensemble deep learning model for splice site prediction. *BMC Bioinformatics*, **23**, 413.

Allbed A, Kumar L, Aldakheel Y Y. 2014. Assessing soil salinity using soil salinity and vegetation indices derived from IKONOS high-spatial resolution imageries: Applications in a date palm dominated region. *Geoderma*, **230**, 1–8.

Angelopoulou T, Tziolas N, Balafoutis A, Zalidis G, Bochtis D. 2019. Remote sensing techniques for soil organic carbon estimation: A review. *Remote Sensing*, **11**, 676.

Ayala Izurieta J E, Jara Santillán C A, Márquez C O, García V J, Rivera-Caicedo J P, Van Wittenberghe S, Delegido J, Verrelst J. 2022. Improving the remote estimation of soil organic carbon in complex ecosystems with Sentinel-2 and GIS using Gaussian processes regression. *Plant and Soil*, **479**, 159–183.

Bashir O, Ali T, Baba Z A, Rather G, Bangroo S, Mukhtar S D, Naik N, Mohiuddin R, Bharati V, Bhat R A. 2021. Soil organic matter and its impact on soil properties and nutrient status. In: *Microbiota and Biofertilizers*. Vol 2: Ecofriendly Tools for Reclamation of Degraded Soil Environs. Springer Nature, Switzerland. pp. 129–159.

Chen B, Huang B, Xu B. 2017. Multi-source remotely sensed data fusion for improving land cover classification. *ISPRS Journal of Photogrammetry and Remote Sensing*, **124**, 27–39.

Curtin D, Beare M H, Hernandez-Ramirez G. 2012. Temperature and moisture effects on microbial biomass and soil organic matter mineralization. *Soil Science Society of America Journal*, **76**, 2055–2067.

Daly E, Porporato A. 2005. A review of soil moisture dynamics: From rainfall infiltration to ecosystem response. *Environmental Engineering Science*, **22**, 9–24.

Dialynas Y G, Bastola S, Bras R L, Billings S A, Markewitz D, Richter D D. 2016. Topographic variability and the influence of soil erosion on the carbon cycle. *Global Biogeochemical Cycles*, **30**, 644–660.

Dong X, Li X, Zheng X, Jiang T, Li X. 2020. Effect of saline soil cracks on satellite spectral inversion electrical conductivity. *Remote Sensing*, **12**, 3392.

Dou X, Wang X, Liu H, Zhang X, Meng L, Pan Y, Yu Z, Cui Y. 2019. Prediction of soil organic matter using multi-temporal satellite images in the Songnen Plain, China. *Geoderma*, **356**, 113896.

Fan M, Lal R, Zhang H, Margenot A J, Wu J, Wu P, Zhang L, Yao J, Chen F, Gao C. 2020. Variability and determinants of soil organic matter under different land uses and soil types in eastern China. *Soil and Tillage Research*, **198**, 104544.

Fu Z, Li Z, Cai C, Shi Z, Xu Q, Wang X. 2011. Soil thickness effect on hydrological and erosion characteristics under sloping lands: A hydropedological perspective. *Geoderma*, **167**, 41–53.

Goidts E, Van Wesemael B, Crucifix M. 2009. Magnitude and sources of uncertainties in soil organic carbon (SOC) stock assessments at various scales. *European Journal of Soil Science*, **60**, 723–739.

Gu Z, Xie Y, Gao Y, Ren X, Cheng C, Wang S. 2018. Quantitative assessment of soil productivity and predicted impacts of water erosion in the black soil region of northeastern China. *Science of the Total Environment*, **637**, 706–716.

Guo H, Fan B, Pan C. 2021. Study on mechanisms underlying changes in agricultural carbon emissions: A case in Jilin Province, China, 1998–2018. *International Journal of Environmental Research and Public Health*, **18**, 919.

Hayward H, Wadleigh C. 1949. Plant growth on saline and alkali soils. *Advances in Agronomy*, **1**, 1–38.

Heikkinen J, Keskinen R, Regina K, Honkanen H, Nuutinen V. 2021. Estimation of carbon stocks in boreal cropland soils-methodological considerations. *European Journal of Soil Science*, **72**, 934–945.

Henderson T, Baumgardner M, Franzmeier D, Stott D, Coster D. 1992. High dimensional reflectance analysis of soil organic matter. *Soil Science Society of America Journal*, **56**, 865–872.

Khan N M, Rastoskuev V V, Sato Y, Shiozawa S. 2005. Assessment of hydrosaline land degradation by using a simple approach of remote sensing indicators. *Agricultural Water Management*, **77**, 96–109.

Kong D, Chu N, Luo C, Liu H. 2024. Analyzing spatial distribution and influencing factors of soil organic matter in cultivated land of northeast China: Implications for black soil protection. *Land*, **13**, 1028.

Lehmann J, Kleber M. 2015. The contentious nature of soil organic matter. *Nature*, **528**, 60–68.

Lesk C, Rowhani P, Ramankutty N. 2016. Influence of extreme weather disasters on global crop production. *Nature*, **529**, 84–87.

Li D, Chen X, Peng Z, Chen S, Chen W, Han L, Li Y. 2012. Prediction of soil organic matter content in a litchi orchard of South China using spectral indices. *Soil and Tillage Research*, **123**, 78–86.

Luo C, Zhang W, Zhang X, Liu H. 2023. Mapping soil organic matter content using Sentinel-2 synthetic images at different time intervals in Northeast China. *International Journal of Digital Earth*, **16**, 1094–1107.

Luo C, Zhang W, Zhang X, Liu H. 2024. Mapping the soil organic matter content in a typical black-soil area using optical data, radar data and environmental covariates. *Soil and Tillage Research*, **235**, 105912.

Luo C, Zhang X, Meng X, Zhu H, Ni C, Chen M, Liu H. 2022. Regional

mapping of soil organic matter content using multitemporal synthetic Landsat 8 images in Google Earth Engine. *Catena*, **209**, 105842.
Lyu X, Li X, Gong J, Li S, Dou H, Dang D, Xuan X, Wang H. 2021. Remote-sensing inversion method for aboveground biomass of typical steppe in Inner Mongolia, China. *Ecological Indicators*, **120**, 106883.
Matinfar H R, Maghsodi Z, Mousavi S R, Rahmani A. 2021. Evaluation and prediction of topsoil organic carbon using machine learning and hybrid models at a field-scale. *Catena*, **202**, 105258.
Nelson D W, Sommers L. 1974. A rapid and accurate procedure for estimation of organic carbon in soils. *Proceedings of the Indiana Academy of Science*, **84**, 456–462.
O'Kelly B C. 2004. Accurate determination of moisture content of organic soils using the oven drying method. *Drying Technology*, **22**, 1767–1776.
Pan Y, Zhang X, Liu H, Wu D, Dou X, Xu M, Jiang Y. 2022. Remote sensing inversion of soil organic matter by using the subregion method at the field scale. *Precision Agriculture*, **23**, 1813–1835.
Paul D, Lade H. 2014. Plant-growth-promoting rhizobacteria to improve crop growth in saline soils: A review. *Agronomy for Sustainable Development*, **34**, 737–752.
Peng S. 2020. *1-km Monthly Precipitation Dataset for China* (*1901–2020*). National Tibetan Plateau Data Center, Beijing, China. (in Chinese)
Peng S, Ding Y, Liu W, Li Z. 2019. 1 km monthly temperature and precipitation dataset for China from 1901 to 2017. *Earth System Science Data*, **11**, 1931–1946.
Post J, Hattermann F F, Krysanova V, Suckow F. 2008. Parameter and input data uncertainty estimation for the assessment of long-term soil organic carbon dynamics. *Environmental Modelling & Software*, **23**, 125–138.
Qin C Z, Zhu A X, Qiu W L, Lu Y J, Li B L, Pei T. 2012. Mapping soil organic matter in small low-relief catchments using fuzzy slope position information. *Geoderma*, **171**, 64–74.
Richardson A D, Jenkins J P, Braswell B H, Hollinger D Y, Ollinger S V, Smith M L. 2007. Use of digital webcam images to track spring green-up in a deciduous broadleaf forest. *Oecologia*, **152**, 323–334.
Sanginga N, Woomer P L. 2009. *Integrated Soil Fertility Management in Africa*: *Principles*, *Practices*, *and Developmental Process*. International Centre for Tropical Agriculture (CIAT), Kenya.
Scharlemann J P, Tanner E V, Hiederer R, Kapos V. 2014. Global soil carbon: Understanding and managing the largest terrestrial carbon pool. *Carbon Management*, **5**, 81–91.
Schillaci C, Acutis M, Lombardo L, Lipani A, Fantappie M, Märker M, Saia S. 2017. Spatio-temporal topsoil organic carbon mapping of a semi-arid Mediterranean region: The role of land use, soil texture, topographic indices and the influence of remote sensing data to modelling. *Science of the Total Environment*, **601**, 821–832.
Segarra J, Buchaillot M L, Araus J L, Kefauver S C. 2020. Remote sensing for precision agriculture: Sentinel-2 improved features and applications. *Agronomy*, **10**, 641.
Shafizadeh-Moghadam H, Minaei F, Talebi-khiyavi H, Xu T, Homaee M. 2022. Synergetic use of multi-temporal Sentinel-1, Sentinel-2, NDVI, and topographic factors for estimating soil organic carbon. *Catena*, **212**, 106077.
Shah S H, Angel Y, Houborg R, Ali S, McCabe M F. 2019. A random forest machine learning approach for the retrieval of leaf chlorophyll content in wheat. *Remote Sensing*, **11**, 920.
Sihi D, Inglett P W, Inglett K S. 2016. Carbon quality and nutrient status drive the temperature sensitivity of organic matter decomposition in subtropical peat soils. *Biogeochemistry*, **131**, 103–119.
Song X D, Brus D J, Liu F, Li D C, Zhao Y G, Yang J L, Zhang G L. 2016. Mapping soil organic carbon content by geographically weighted regression: A case study in the Heihe River Basin, China. *Geoderma*, **261**, 11–22.
Tian L, Wu X, Tao Y, Li M, Qian C, Liao L, Fu W. 2023. Review of remote sensing-based methods for forest aboveground biomass estimation: Progress, challenges, and prospects. *Forests*, **14**, 1086.
Tian Y, Zhang J, Yao X, Cao W, Zhu Y. 2013. Laboratory assessment of three quantitative methods for estimating the organic matter content of soils in China based on visible/near-infrared reflectance spectra. *Geoderma*, **202**, 161–170.
Wang L, Liu H, Wang X, Xu X, He L, Luo C, Li Y, Zhang X, Zang D, Zheng S. 2025. Identifying optimal variables to predict soil organic carbon in sandy, saline, and black soil regions: Remote sensing, terrain, or climate factors? *Remote Sensing*, **17**, 237.
Wang X, Han J, Wang X, Yao H, Zhang L. 2021. Estimating soil organic matter content using Sentinel-2 imagery by machine learning in Shanghai. *IEEE Access*, **9**, 78215–78225.
Wang X, Wang L, Li S, Wang Z, Zheng M, Song K. 2022. Remote estimates of soil organic carbon using multi-temporal synthetic images and the probability hybrid model. *Geoderma*, **425**, 116066.
Wang Y, Luo C, Zhang W, Meng X, Liu Q, Zhang X, Liu H. 2022. Remote sensing prediction model of cultivated land soil organic matter considering the best time window. *Sustainability*, **15**, 469.
Wang Z, Ding J, Zhang Z. 2022. Estimation of soil organic matter in arid zones with coupled environmental variables and spectral features. *Sensors*, **22**, 1194.
Williams P. 1987. Variables affecting near-infrared reflectance spectroscopic analysis. In: *Near-infrared Technology in the Agricultural and Food Industries*. American Association of Cereal Chemists St. Paul, Minnesota, USA. pp. 143–167.
Xie Y, Chen T B, Lei M, Yang J, Guo Q J, Song B, Zhou X Y. 2011. Spatial distribution of soil heavy metal pollution estimated by different interpolation methods: Accuracy and uncertainty analysis. *Chemosphere*, **82**, 468–476.
Yang Y, Chen R, Liu G, Liu Z, Wang X. 2022. Trends and variability in snowmelt in China under climate change. *Hydrology and Earth System Sciences*, **26**, 305–329.
You N, Dong J. 2020. Examining earliest identifiable timing of crops using all available Sentinel 1/2 imagery and Google Earth Engine. *ISPRS Journal of Photogrammetry and Remote Sensing*, **161**, 109–123.
Yu H, Zha T, Zhang X, Nie L, Ma L, Pan Y. 2020. Spatial distribution of soil organic carbon may be predominantly regulated by topography in a small revegetated watershed. *Catena*, **188**, 104459.
Yu L, Yang J, Bu K, Liu T, Jiao Y, Li G, Pu L, Zhang S. 2021. Impacts of saline-alkali land improvement on regional climate: Process, mechanisms, and implications. *Remote Sensing*, **13**, 3407.
Zeglin L H, Bottomley P J, Jumpponen A, Rice C, Arango M, Lindsley A, McGowan A, Mfombep P, Myrold D. 2013. Altered precipitation regime affects the function and composition of soil microbial communities on multiple time scales. *Ecology*, **94**, 2334–2345.
Zhang M, Zhang M, Yang H, Jin Y, Zhang X, Liu H. 2021. Mapping regional soil organic matter based on Sentinel-2A and modis imagery using machine learning algorithms and google earth engine. *Remote Sensing*, **13**, 2934.
Zhao W, Zhou C, Zhou C, Ma H, Wang Z. 2022. Soil salinity inversion model of oasis in arid area based on UAV multispectral remote sensing. *Remote Sensing*, **14**, 1804.
Zhao X, Zhang Z, Zhao M, Song X, Liu X, Zhang X. 2023. The quantified and major influencing factors on spatial distribution of soil organic matter in provincial-scale farmland — a case study of Shandong Province in eastern China. *Applied Sciences*, **13**, 3738.
Zhou J, Liu C, Shi L, Zamanian K. 2024. Rhizosphere influence on microbial functions: Consequence for temperature sensitivity of soil organic matter decomposition at early stage of plant growth. *Plant and Soil*, **494**, 95–109.
Zhou X, Lu P, Zheng Z, Tolliver D, Keramati A. 2020. Accident prediction accuracy assessment for highway-rail grade crossings using random forest algorithm compared with decision tree. *Reliability Engineering & System Safety*, **200**, 106931.
Žížala D, Minařík R, Zádorová T. 2019. Soil organic carbon mapping using multispectral remote sensing data: Prediction ability of data with different spatial and spectral resolutions. *Remote Sensing*, **11**, 2947.
Zou J, Wei Y, Zhang Y, Liu Z, Gai Y, Chen H, Liu P, Song Q. 2024. Remote sensing inversion of soil organic matter in cropland combining topographic factors with spectral parameters. *Frontiers in Environmental Science*, **12**, 1420557.

Executive Editor-in-Chief Jinshui Wu
Managing Editor Lujuan Sun